Background estimation in nonlinear image restoration

Geert M. P. van Kempen

Central Analytical Sciences, Unilever Research Vlaardingen, Olivier van Noortlaan 120, 3133 AT Vlaardingen, The Netherlands

Lucas J. van Vliet

Pattern Recognition Group, Faculty of Applied Sciences, Delft University of Technology, Lorentzweg 1, 2628 CJ Delft, The Netherlands

Received March 4, 1999; revised manuscript received August 23, 1999; accepted November 8, 1999

One of the essential ways in which nonlinear image restoration algorithms differ from linear, convolution-type image restoration filters is their capability to restrict the restoration result to nonnegative intensities. The iterative constrained Tikhonov–Miller (ICTM) algorithm, for example, incorporates the nonnegativity constraint by clipping all negative values to zero after each iteration. This constraint will be effective only when the restored intensities have near-zero values. Therefore the background estimation will have an influence on the effectiveness of the nonnegativity constraint of these algorithms. We investigated quantitatively the dependency of the performance of the ICTM, Carrington, and Richardson–Lucy algorithms on the estimation of the background and compared it with the performance of the linear Tikhonov–Miller restoration filter. We found that the performance depends critically on the background estimation: An underestimation of the background will make the nonnegativity constraint ineffective, which results in a performance that does not differ much from the Tikhonov–Miller filter performance. A (small) overestimation, however, degrades the performance dramatically, since it results in a clipping of object intensities. We propose a novel general method to estimate the background based on the dependency of nonlinear restoration algorithms on the background, and we demonstrate its applicability on real confocal images.
[S0740-3232(00)00803-6]

OCIS codes: 100.1830, 100.3020, 100.6890, 180.1490, 180.6900, 180.1520.

1. INTRODUCTION

One of the essential ways in which nonlinear image restoration algorithms such as the iterative constrained Tikhonov–Miller algorithm[1,2] (ICTM), the Carrington algorithm,[3,4] and the Richardson–Lucy algorithm[5–12] differ from linear convolution-type image restoration filters is their capability to restrict the restoration result to nonnegative intensities. This property has been linked to the so-called superresolution property of these algorithms[4,13–15]—the capability to (partially) restore information outside the bandwidth of the optical transfer function.

The ICTM algorithm, for example, incorporates the nonnegativity constraint by clipping all negative values to zero after each iteration of the conjugate-gradient-descent algorithm used to minimize the Tikhonov–Miller functional. This constraint will be effective only when the intensities of the iterations have near-zero values. We model the image formation in a confocal microscope as the convolution of the original image with the microscope's point-spread function on a background and distorted by noise.[6,11]

The ICTM and Carrington algorithms subtract the estimated background from the first estimate before they start the iteration. Therefore the background estimation will have an influence on the effectiveness of the nonnegativity constraint of these algorithms. We investigate the effect of the background estimation on the performance of the ICTM, Carrington, and Richardson–Lucy algorithms and on the performance of the Tikhonov–Miller regularized expectation-maximization–maximum-likelihood-estimator (EM–MLE) algorithm (as proposed by Conchello *et al.*),[16] and we compare the performance of the nonlinear methods with the performance of the linear Tikhonov–Miller restoration filter.[17]

The removal of the background from the acquired image is incorporated differently in the investigated algorithms. In the Tikhonov–Miller, ICTM, and Carrington algorithms the assumption of additive Gaussian noise removes the dependency of the noise from the object and background. Therefore the background can be removed by subtracting it from the acquired image. The Richardson–Lucy and Conchello algorithms model the noise as Poisson noise. This prevents the removal of the background by a simple subtraction. Instead, the background is incorporated into the conditional expectation of the translated Poisson process used to model the object intensities in the image. The EM algorithm uses the relative weights of the intensity of the object and of the background to estimate the object intensity from the intensities found in the acquired image.

In both approaches an overestimation of the background will lead to large errors in the estimation of the object intensity. In the case of the ICTM and Carrington

algorithms the subtraction of an overestimated background reduces low object intensities to negative values, which are clipped to zero after the first iteration. This leads to an incorrect estimation of the object's shape and reduces the performance of the algorithm. Similarly, an overestimation of the background in the EM case will lead to an underestimation of the object's intensities and thus produce a poor performance.

An underestimation of the background yields undesired properties, as well. Not only will it lead to an incomplete removal of the background, but, in the case of the ICTM and Carrington algorithms, low object intensities will not be set to near-zero values in the first estimate. Therefore the number of points in the object that are being clipped after each iteration is considerably reduced. Since the clipping operation of these algorithms is the only nonlinear operation that distinguishes them from the linear Tikhonov–Miller filter, a substantial reduction of the number of pixels being clipped will decrease the effectiveness of the nonnegativity constraint and therefore the performance benefits of these algorithms.

In the extreme case where no points are being set to zero, both the ICTM and the Carrington algorithms reduce to an iterative conjugate-gradient algorithm, producing a solution that is identical to the one produced by the linear Tikhonov–Miller restoration filter. In other words, without clipping, the ICTM and Carrington algorithms produce a solution equal to the linear solution, thus without restoring information beyond the bandwidth of the point-spread function. In that case the ICTM and Carrington algorithms will not produce the sometimes claimed "superresolution" results.

Although the performance decrease of nonlinear restoration algorithms to linear performance caused by a severe underestimation of the background has been reported before,[18] in this paper we quantify this dependence and show the critical dependency of the performance of these algorithms on the actual background estimation. Furthermore, we propose a novel general method for estimating the background and demonstrate its applicability on real confocal images.

In Section 2 we derive, on the basis of a linear model for image formation, the linear Tikhonov–Miller restoration algorithm and the four nonlinear image restoration algorithms. In Section 3 we describe how we performed our simulation experiments; in Section 4 we present the results of these experiments. On the basis of these results, in Section 5 we propose a novel method for the estimation of the background. We conclude in Section 6.

2. IMAGE RESTORATION

A. Classical Image Restoration: The Tikhonov–Miller Restoration Filter

We assume that the image formation in a confocal fluorescence microscope can be modeled as a linear translation-invariant system distorted by noise:

$$m(x,y,z) = N[h(x,y,z) \otimes f(x,y,z) + b(x,y,z)]. \quad (1)$$

In this equation, f represents the input signal, h the point-spread function, b a (constant) background signal, N a general noise-distortion function, and m the recorded fluorescence image. For scientific-grade light detectors, N is dominated by Poisson noise.[19,20] In classical image restoration, the signal-dependent Poisson noise is approximated by additive Gaussian noise. Using this additive Gaussian noise model for N, we rewrite Eq. (1) as

$$\begin{aligned} g(x,y,z) &= m(x,y,z) - b(x,y,z) \\ &= h(x,y,z) \otimes f(x,y,z) + n(x,y,z). \end{aligned} \quad (2)$$

After sampling, Eq. (2) becomes

$$\begin{aligned} g[x,y,z] = \sum_{i=1}^{M_x} \sum_{j=1}^{M_y} \sum_{k=1}^{M_z} & h(x-i, y-j, z-k) \\ & \times f(i,j,k) + n(x,y,z), \end{aligned} \quad (3)$$

with M_x, M_y, and M_z the number of sampling points in the x, y, and z dimensions, respectively. For convenience we will adopt a matrix notation,

$$\mathbf{g} = \mathbf{H}\mathbf{f} + \mathbf{n}, \quad (4)$$

where the vectors $\mathbf{f}$, $\mathbf{g}$, and $\mathbf{n}$ of length M ($M = M_x M_y M_z$) denote the object, its image, and the additive Gaussian noise, respectively. The $M \times M$ matrix $\mathbf{H}$ is the blurring matrix representing the point-spread function of the microscope.

The Tikhonov–Miller filter, a classical image restoration filter, is a convolution filter operating on the measured image. It can be written as

$$\hat{\mathbf{f}} = \mathbf{W}\mathbf{g} \quad (5)$$

with $\mathbf{W}$ the linear restoration filter and $\hat{\mathbf{f}}$ its result. The Tikhonov–Miller filter is derived from a least-squares approach,[14] which is based on minimizing the well-known Tikhonov functional[21]

$$\Phi(\hat{\mathbf{f}}) = \|\mathbf{H}\hat{\mathbf{f}} - \mathbf{g}\|^2 + \lambda \|\mathbf{C}\hat{\mathbf{f}}\|^2, \quad (6)$$

with $\|\cdot\|^2$ the Euclidean norm. In image restoration λ is known as the regularization parameter and $\mathbf{C}$ as the regularization matrix. The Tikhonov functional consists of a mean-square-error fitting criterion and a stabilizing energy bound that penalizes solutions of $\hat{\mathbf{f}}$ that oscillate wildly as a result of spectral components that are dominated by noise. The minimum of Φ yields the well-known Tikhonov–Miller (denoted TM) solution $\mathbf{W}_{\mathrm{TM}}$

$$\mathbf{W}_{\mathrm{TM}} = (\mathbf{H}^T\mathbf{H} + \lambda \mathbf{C}^T\mathbf{C})^{-1}\mathbf{H}^T. \quad (7)$$

The convolution nature of the Tikhonov–Miller restoration filter makes it incapable of restoring spatial frequencies for which the optical transfer function (OTF) has zero transmission. In particular, the OTF of a three-dimensional (3-D) conventional fluorescence microscope has large regions with zero response known as the missing cone.[22]

Furthermore, convolution methods cannot restrict the domain in which the solution should be found. This property is a major drawback since the intensity of an imaged object represents light energy, which is nonnegative. Finally, Van der Voort[2] showed that the Tikhonov–Miller filter is very sensitive to errors in the estimation of the point-spread function, which cause ringing artifacts.

The ICTM algorithm, the Carrington algorithm, and the Richardson–Lucy algorithm are frequently used in fluorescence microscopy.[2,3,5,6,16,23,24] These iterative nonlinear algorithms tackle the above-mentioned problems at a cost of a considerable increase in the computational complexity. Such algorithms require a large number of iterations, each with a complexity comparable to that of the Tikhonov–Miller filter.

B. Constrained Tikhonov Restoration

1. Iterative Constrained Tikhonov–Miller Algorithm

The iterative constrained Tikhonov–Miller[1,2,25] (ICTM) algorithm finds the minimum of Eq. (6) with the method of conjugate gradients.[26] The nonnegativity constraint is incorporated by setting the negative intensities to zero after each iteration.

2. Carrington Algorithm

Like the ICTM algorithm, the Carrington algorithm[3,4] minimizes the Tikhonov functional under the constraint of nonnegativity. However, the algorithm is based on a more solid mathematical foundation.

Using the Kuhn–Tucker conditions,

$$\nabla_{\hat{\mathbf{f}}}\Phi_i = 0 \quad \text{and} \quad \hat{\mathbf{f}}_i > 0 \quad \text{or} \quad \nabla_{\hat{\mathbf{f}}}\Phi_i \geqslant 0 \quad \text{and} \quad \hat{\mathbf{f}}_i = 0, \quad (8)$$

Carrington[3,4,27] and co-workers transformed the Tikhonov functional (6) with the added nonnegativity constraint to the Ψ (on the set $\mathbf{H}^T\mathbf{c} > 0$):

$$\Psi(\mathbf{c}) = \tfrac{1}{2}\,\|P(\mathbf{H}^T\mathbf{c})\|^2 - \mathbf{c}^T\mathbf{g} + \tfrac{1}{2}\,\lambda\|\mathbf{c}\|^2. \quad (9)$$

Since Ψ is strictly convex and twice continuously differentiable, a conjugate-gradient algorithm can be used to minimize Ψ (Ref. 26) (Ψ is strictly convex since its second derivative is positive definite[3]).

C. Maximum-Likelihood Restoration: The Richardson–Lucy Algorithm

In contrast to the two algorithms discussed above, the Richardson–Lucy algorithm is not derived from the image formation model [Eq. (4)], which assumes additive Gaussian noise. Instead, the general noise-distortion function N is assumed to be dominated by Poisson noise.

A fluorescence object can be modeled as a spatially inhomogeneous Poisson process $\mathbf{F}$ with an intensity function $\mathbf{f}$ (Ref. 28):

$$P(\mathbf{F}_i|\mathbf{f}_i) = \frac{\mathbf{f}_i^{\mathbf{F}_i}\exp(-\mathbf{f}_i)}{\mathbf{F}_i!}.$$

The image formation of such an object by a fluorescence microscope can be modeled as a translated Poisson process.[28] This process models the transformation of $\mathbf{F}$ into a Poisson process $\mathbf{m}$ subjected to a conditional probability density function $\mathbf{H}$,

$$E[\mathbf{m}] = \mathbf{H}\mathbf{f} + \mathbf{b}, \quad (10)$$

with $\mathbf{b}$ the mean of an independent (background) Poisson process. The conditional probability density function is in this case the point-spread function of the fluorescence microscope. The log-likelihood function of such a Poisson process is given by[28]

$$L(\mathbf{f}) = -\sum \mathbf{H}\mathbf{f} + \mathbf{m}^T\ln(\mathbf{H}\mathbf{f} + \mathbf{b}), \quad (11)$$

where we have dropped all terms that are not dependent on $\mathbf{f}$. The maximum of the likelihood function L can be found iteratively by using the EM algorithm.[7] This iterative algorithm was first used by Vardi *et al.*[8] in emission tomography. Holmes[5] introduced the algorithm to microscopy. Applying the EM algorithm to Eq. (11) yields[5,6,9–11]

$$\hat{\mathbf{f}}^{k+1} = \hat{\mathbf{f}}^k\mathbf{H}^T\left[\frac{\mathbf{m}}{\mathbf{H}\hat{\mathbf{f}}^k + \mathbf{b}}\right]. \quad (12)$$

The EM algorithm ensures a nonnegative solution when a nonnegative initial guess $\hat{\mathbf{f}}^0$ is used. Furthermore, the likelihood of each iteration of the EM algorithm will strictly increase to a global maximum.[28] The EM algorithm for finding the maximum-likelihood estimator of a translated Poisson process (often referred to as EM–MLE) is identical to the Richardson–Lucy algorithm.[12]

The Richardson–Lucy algorithm is a constrained but unregularized iterative image restoration algorithm. (Limiting the number of iterations, however, can serve as regularization; see, for example, Ref. 29). The ICTM and Carrington algorithms, however, incorporate Tikhonov regularization to suppress undesired solutions. Conchello has derived an algorithm that incorporates Tikhonov regularization into the Richardson–Lucy algorithm.[16] This incorporation yields the following conditional expectation Q for estimating the intensity of a translated Poisson process[16]:

$$Q(\mathbf{f}|\hat{\mathbf{f}}^k) = -\sum \mathbf{f} + E[\mathbf{F}|\mathbf{m},\hat{\mathbf{f}}^k]^T\ln\mathbf{f} - \alpha\|\mathbf{f}\|^2. \quad (13)$$

The maximization step of the EM algorithm now yields[16]

$$\frac{E[\mathbf{F}|\mathbf{m},\hat{\mathbf{f}}^k]}{\hat{\mathbf{f}}^{k+1}_{\text{regularized}}} - 2\alpha\hat{\mathbf{f}}^{k+1}_{\text{regularized}} - 1 = 0. \quad (14)$$

This quadratic equation in $\hat{\mathbf{f}}^{k+1}_{\text{regularized}}$ can be solved with the Euler equation for variational calculus,[16] which yields

$$\hat{\mathbf{f}}^{k+1}_{\text{regularized}} = \frac{-1 + (1 + 2\lambda\hat{\mathbf{f}}^{k+1})^{1/2}}{\lambda}, \quad (15)$$

with regularization parameter $\lambda = 4\alpha$ and $\hat{\mathbf{f}}^{k+1}$ given by Eq. (12). With use of l'Hopital's rule, it is easy to show that Eq. (15) becomes Eq. (12) when $\lambda \to 0$. We will refer to this algorithm as the RL–Conchello algorithm.

3. EXPERIMENTS

In this section we present results from a simulation experiment in which the performance of several image restoration algorithms is measured as a function of the estimated background. We measured not only the overall performance but also the performance in specific regions of both the frequency and the spatial domains. We used

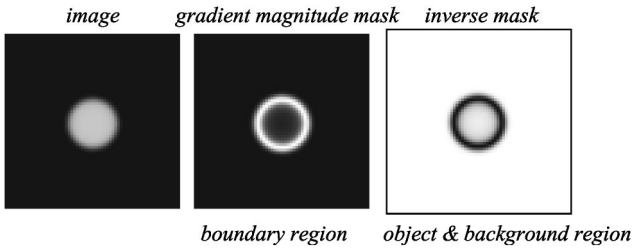

Fig. 1. Generation of object, boundary, and background region gray-weighted masks with use of the gradient magnitude of the image.

the footprint of the OTF[22] as a mask to measure the performance inside and outside the bandwidth of the point-spread function. This gives insight to what extent these nonlinear algorithms restore information beyond the microscope's resolution.

In the spatial domain we measured the performance in three regions in the image: inside the object, at its boundary, and in the background of the image. To avoid aliasing effects, we used band-limited masks to select these regions. The mask for the boundary region was generated by normalizing the gradient magnitude of the acquired image (see Fig. 1). We computed the gradient of the image by convolving the image with Gaussian derivatives, and we used a sigma of 0.9 pixels for the derivatives. We segmented the inverse of the boundary mask into two masks: an object mask and a background mask (see Fig. 1).

We tested the linear Tikhonov–Miller filter, the ICTM algorithm, the Carrington algorithm, the Richardson–Lucy algorithm, and the RL–Conchello algorithm. We included the ICTM algorithm without clipping after each iteration to show that this variant of the ICTM algorithm is nothing but a conjugate-gradient algorithm for obtaining the linear Tikhonov–Miller result. The ICTM algorithm performs better than linear filters owing to the clipping after each iteration. One could question whether the result obtained in this way is different from that from clipping the result of the linear Tikhonov–Miller filter. We have therefore included the result of this procedure as well (referred to as clipped Tikhonov–Miller).

All images were generated with the same constant background intensity of 16.0 arbitrary digital units (ADU). However, we varied the estimate of the background intensity, which is an input to the restoration algorithms, from 0.0 to 32.0 ADU. We have used a simulated confocal point-spread function with a NA of 1.3, a refractive index of 1.515, an excitation wavelength of 488 nm, an emission wavelength of 520 nm, and a pinhole diameter of 300 nm. The images, sampled at twice the Nyquist rate, are $64 \times 64 \times 32$ pixels large, which corresponds to an image size of $1.55 \times 1.55 \times 2.73\ \mu$m. We used spheres with an intensity of 200.0 ADU and a diameter of 500 nm as objects. In this experiment we used a signal-to-noise ratio of 1.0, which corresponds to a conversion factor of 0.22 ADU/photon.

4. RESULTS

Figures 2 and 3 clearly show that the performance of the tested nonlinear restoration algorithms is strongly dependent on the estimation of the background. A (severe) underestimation of the background yields a performance of these algorithms that is not significantly better than that of the linear Tikhonov–Miller filter. An overestimation has an even more dramatic influence on the performance. The performance drops quite significantly for relatively small overestimations (<25%), drops below the performance of the linear filter for an overestimation of 25–50%, and even drops below the performance of the unrestored (acquired) image for an overestimation larger

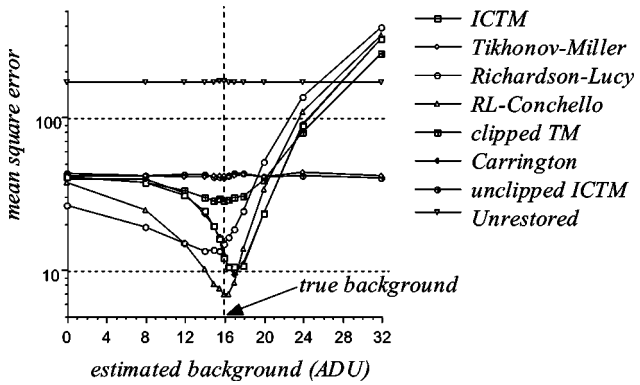

Fig. 2. Mean-square-error performance of the ICTM, Tikhonov–Miller, Richardson–Lucy, RL–Conchello, clipped Tikhonov–Miller (TM), Carrington, and unclipped ICTM algorithms together with the performance of the unrestored data as a function of the estimated background value.

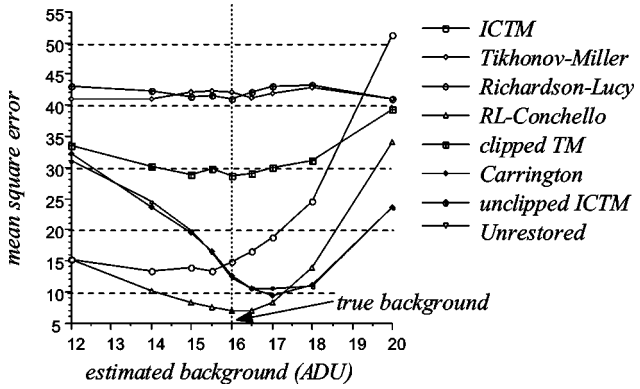

Fig. 3. Enlargement of Fig. 2 around the true background.

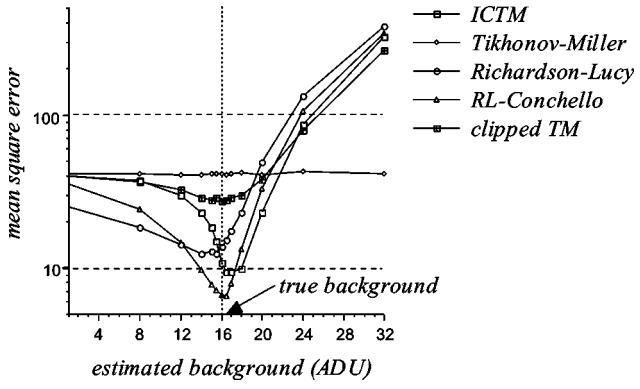

Fig. 4. Mean-square-error performance of the ICTM, Tikhonov–Miller, Richardson–Lucy, RL–Conchello, and clipped TM algorithms measured inside the bandwidth of the OTF.

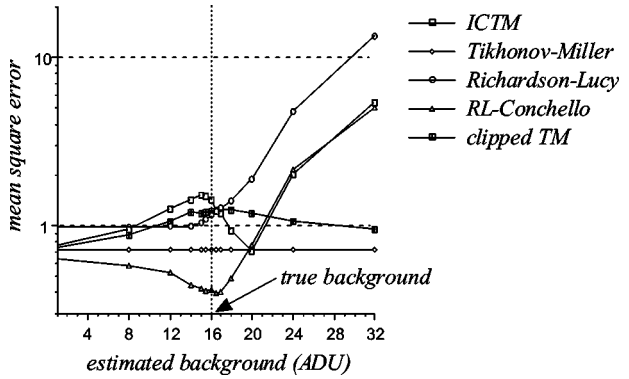

Fig. 5. Mean-square-error performance of the ICTM, Tikhonov–Miller, Richardson–Lucy, RL–Conchello, and clipped TM algorithms measured outside the bandwidth of the OTF.

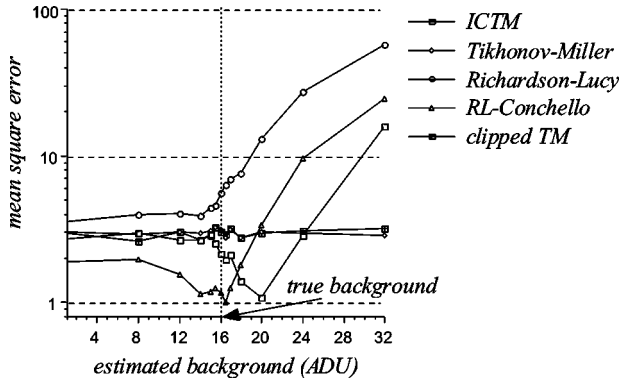

Fig. 6. Mean-square-error performance of the ICTM, Tikhonov–Miller, Richardson–Lucy, RL–Conchello, and clipped TM algorithms measured inside the object.

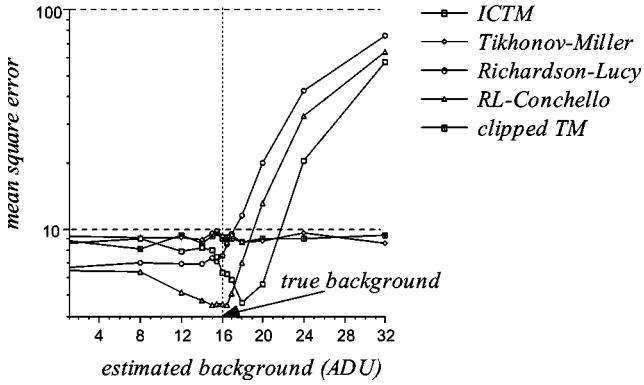

Fig. 7. Mean-square-error performance of the ICTM, Tikhonov–Miller, Richardson–Lucy, RL–Conchello, and clipped TM algorithms measured around the edges of the object.

than 50%. (A lower performance corresponds to a higher mean square error, which is plotted in Fig. 4).

The figures also show that the performance of the unclipped ICTM is identical to that of the linear Tikhonov–Miller filter and that the Carrington algorithm yields a performance characteristic very similar to that of the ICTM algorithm. We have therefore not included the results of the unclipped ICTM algorithm and the Carrington algorithm in further analysis.

The performance inside the bandwidth of the OTF as shown in Fig. 4 shows a characteristic similar to that found for the overall performance. Roughly 90% of the total mean square error is measured in this region. This finding is simply explained by the fact that most of the object energy is found in this region. The remaining 10% found outside the bandwidth of the OTF shows a slightly different characteristic (see Fig. 5).

The mean square error of the linear Tikhonov–Miller algorithm is lower here than all the nonlinear algorithms except the RL–Conchello algorithm. The mean square error of the Tikhonov–Miller filter is simply the energy of the object in this region of the Fourier domain. As expected, the nonlinear algorithms add frequency components outside the bandwidth of the OTF to improve the performance inside the bandwidth. These restored components, however, do not always improve the performance outside the bandwidth as well.

The performance in the spatial domain on the object, edge, and background is shown in Figs. 6, 7, and 8, re-

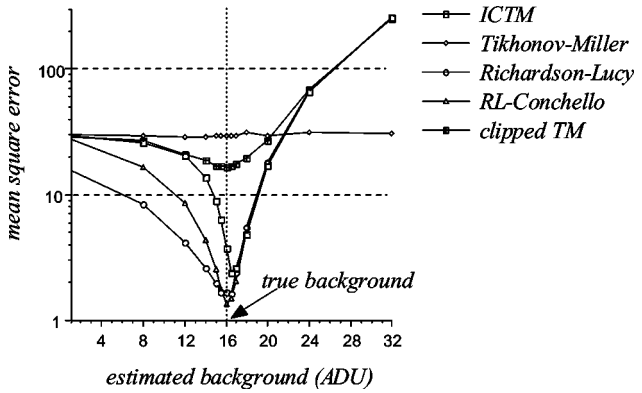

Fig. 8. Mean-square-error performance of the ICTM, Tikhonov–Miller, Richardson–Lucy, RL–Conchello, and clipped TM algorithms measured in the background.

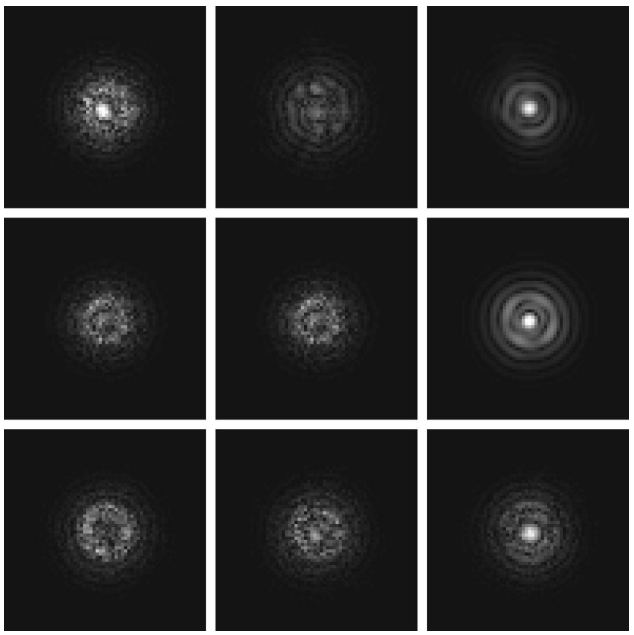

Fig. 9. Mean square error in the center $\omega_x\omega_y$ slice of the ICTM (top), RL–Conchello (middle), and clipped TM (bottom) algorithms for an estimated background of 12.0 (left), 16.0 (center), and 20.0 (right). The gray scaling is constant over all nine images.

spectively. We conclude from these figures that the largest gain in performance is found in the background, the region that contains the most pixels and the lowest pixel intensities.

The ICTM algorithm produces the best performance in the object and edge regions for an overestimation of 12.5–25%, when some of the low-intensity edges of the object are being clipped, thereby introducing (correlated) high-frequency components (see Fig. 5). These figures also show clearly that only the performance of the clipped Tikhonov–Miller algorithm in the background region is influenced by the background estimation. Figure 9 shows the mean square error at every frequency in the center $\omega_x\omega_y$ slice between the original object and the restoration results of the ICTM, RL–Conchello, and clipped Tikhonov–Miller algorithms for three values of the estimated background (12.0, 16.0, and 20.0). It shows clearly that errors due to noise (stochastic errors) are replaced by "deterministic" errors at low frequencies.

5. BACKGROUND ESTIMATION

The experimental results presented in Section 4 show the strong influence of the background estimation on the performance of nonlinear restoration algorithms. In this section we discuss how the background can be estimated in real images.

Given the diversity of the samples being imaged with fluorescence (confocal) microscopy, the characteristics of the acquired images are similarly diverse. Therefore it is impossible to construct a single background-estimation algorithm suitable for such a wide range of images. Not only do the samples vary from sparse (like our images of spheres) to very dense, but the backgrounds can be different as well.

In general, the background can be characterized as being of low intensity and of a low spatial frequency. In images of sparse objects the majority of the pixels are background pixels, and a histogram-based algorithm can be used to estimate the background by fitting a parabola through the maximum values in the histogram. Figure 10 shows the histogram of one of the simulated confocal images used in the experiments described in Section 3. Assuming that the distribution of the dominant noise source in the image is unbiased and unimodal (which holds for Poisson noise), we can estimate the background by using the position of the maximum of the histogram.

In images of dense objects or in images with a nonconstant background, the histogram-based approach will not be very accurate (still, the maximum of the lowest-intensity peak might give a reasonable estimate). In these cases an approach based on mathematical morphology or fitting of a polynomial might work.

In the first approach, an opening operation can be used to estimate the shape of the background.[30] The second approach fits a low-order polynomial through the pixels.[31] The accuracy and the bias of the fit will be improved if the fit is done through background pixels only. Therefore the image needs to be segmented (coarsely) into object and background pixels. One way of doing this is to use a criterion based on the noise variance. Given a first

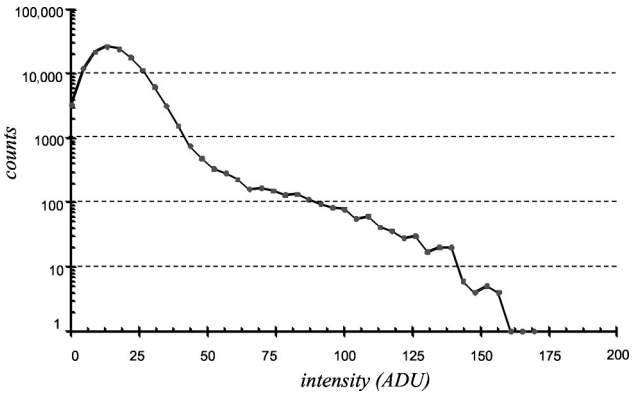

Fig. 10. Histogram of a simulated confocal image as used in the experiment described in Section 3.

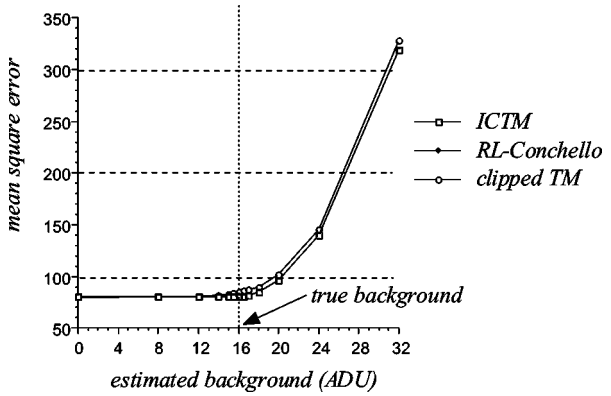

Fig. 11. Mean square error between the acquired image and the blurred restoration result as a function of the background.

(histogram-based) estimate of the background intensity, a pixel can be labeled as object pixel if its intensity is more than n (for example two or three) times the standard deviation of the noise.

We propose, however, an alternative method for estimating the background by using the dependency of the nonlinear restoration algorithms on the background estimation. As illustrated by Fig. 4, the performance of the nonlinear algorithms inside the bandwidth of the OTF is (strongly) dependent on the background. Therefore a measure that uses this part of the frequency domain can be used to measure the performance of a nonlinear algorithm as a function of the background estimation. By optimizing this measure as a function of the background, we can determine the optimal background. We propose to use the mean square error between the acquired image and the restoration result blurred by the microscope's OTF with the added background,

$$\sum [\mathbf{g} - (\mathbf{H}\hat{\mathbf{f}} + \mathbf{b})]^2, \tag{16}$$

to measure the performance as a function of the background. The values of this measure as discussed in the experiments in Section 4 are shown in Fig. 11 for the ICTM, clipped Tikhonov–Miller, RL–Conchello, and Richardson–Lucy algorithms.

Using the proposed measure, we can find the optimal background value by increasing the background value un-

til the mean square error increases significantly. For a constant background, the optimal background value will be found in the interval between zero and the mean intensity of the acquired image.

A disadvantage of the proposed method for background estimation is that it requires a few restoration results obtained with, for example, the ICTM algorithm. This could lead to a high computational complexity, resulting in an unacceptably long processing time. This problem could be solved by using the clipped Tikhonov–Miller filter instead. As can be observed from Fig. 2, the mean square error of the clipped Tikhonov–Miller filter is also minimal for the correct value of the background.

To demonstrate the ability of the proposed method in background estimation, we have applied it to real confocal images. Figure 12 shows an $x-y$ slice of a 3-D confocal image of a monoglyceride.[32,33] This monoglyceride has been used as an alternative to fat in structuring water in margarinelike spreads. The monoglyceride forms a microscopic house-of-cards-like structure in which the water is contained. The monoglycerides have been stained with Nile Red and are excited at a wavelength of 488 nm, and the emitted light has been measured at 522 nm. The image is $256 \times 256 \times 256$ pixels in size, sampled at 50 nm laterally and axially. The histogram of this image, shown in Fig. 13, reveals that the image is dominated by a broad distribution of low intensities, which makes estimation of the background from the histogram difficult. We have measured the values of the proposed discrepancy function [Eq. (16)] for the clipped Tikhonov–Miller, the ICTM, and the RL–Conchello algorithms as a function of the background; see Fig. 14.

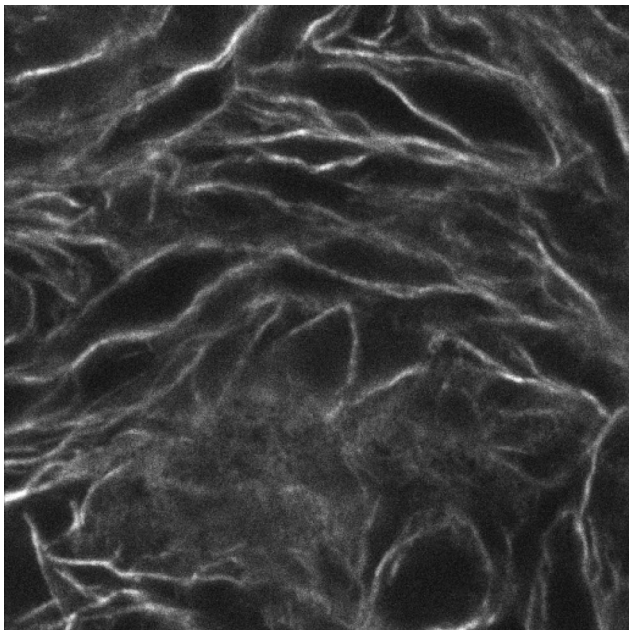

Fig. 12. $X-Y$ slice of a 3-D confocal image of a monoglyceride stained with Nile Red.

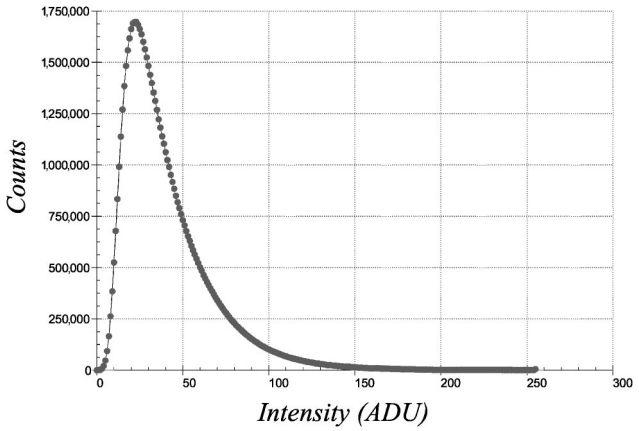

Fig. 13. Histogram of the 3-D confocal images shown in Fig. 12.

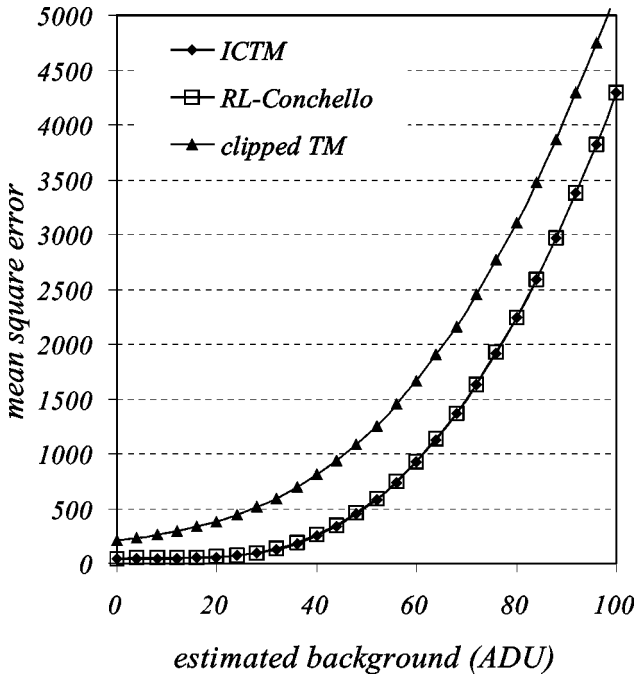

Fig. 14. Plot of the proposed discrepancy function for background estimation as a function of the background for the clipped TM, ICTM, and RL–Conchello algorithms.

6. DISCUSSION AND CONCLUSIONS

We modeled the deterministic part of the image formation as a convolution of the original object with the point-spread function on a background. Since we required that restoration algorithms restore the original object from the acquired image, both the blurring and the background needed to be removed from the image. The iterative restoration algorithms discussed in this paper are nonlinear, since they constrain their results to nonnegative values. This constraint will be effective only when the intensities in the restoration result have values near zero. We have shown that the effectiveness of this constraint is strongly influenced by the background estimation, which is an input parameter in all restoration algorithms. We have shown that a modest ($> \sim 50\%$) underestimation of the background will make the constraint ineffective, which results in a performance of these nonlinear algorithms that does not differ much from the performance obtained by linear restoration filters. A small ($> \sim 25\%$) overestimation of the background, however, is even more dramatic, since it results in a clipping of object intensities.

We have showed that this clipping dramatically degrades the performance of these nonlinear restoration algorithms. In the simulation experiments presented, we used only a single type of object, a solid sphere. It could be argued that this precludes general conclusions regarding the dependency of the performance of nonlinear restoration algorithms on the background estimation. However, the restoration algorithms tested do not use explicit knowledge of the objects, and simulation experiments that measured the performance of these algorithms as a function of parameters, such as the signal-to-noise ratio and regularization parameters, show a similar behavior of these algorithms for different objects.[6,34] Finally, the experimental data shown in Section 4 confirm the simulation results.

We have investigated the ICTM, Carrington, and Richardson–Lucy algorithms in this paper. Although these algorithms are frequently used in fluorescence microscopy, they are by no means the only existing nonlinear restoration algorithms. See, for example, Refs. 18, 24, and 35 for an overview of alternative algorithms. It is beyond the scope of this paper to investigate the dependence on the background estimation of all these algorithms; nevertheless, we believe that we have addressed a general issue that should be investigated before a particular nonlinear algorithm is used.

Finally, we proposed a novel general method to estimate the background based on the dependence of the performance of these nonlinear restoration algorithms on the background. We have demonstrated the applicability of this method on real confocal images. The object used in the simulation differs significantly from the type of sample used in experiments with real data. Nevertheless, the proposed discrepancy function shows similar behavior on both the simulated and the real data. This indicates, in our opinion, that the proposed method for estimating the background is a general one, applicable to a wide range of images.

The proposed method relies on a determination of the background value for which the discrepancy between the original image and the reblurred restoration results increases significantly. The problem of finding the optimal value cannot easily be incorporated in a standard numerical optimization procedure such as searching for an extremum or a zero crossing (although the optimal value would coincide with a maximum of the second derivative, this is probably too noisy to be robust). A possible way to detect the optimal background value is to set a threshold on the increase in the discrepancy function and then set the value of the background for which this threshold is reached as the optimal value. The threshold value could be a percentage of the offset discrepancy (the discrepancy at very low background values), and the percentage itself is related to the amount of noise in the image. What the relation is between this percentage and the signal-to-noise ratio could be investigated in future research.

ACKNOWLEDGMENT

This work was partially supported by the Royal Netherlands Academy of Arts and Sciences (KNAW) and by the Rolling Grants program of the Foundation for Fundamental Research in Matter (FOM).

REFERENCES

1. R. L. Lagendijk and J. Biemond, *Iterative Identification and Restoration of Images, Vol. IP* (Kluwer Academic, Dordrecht, The Netherlands, 1991).
2. H. T. M. van der Voort and K. C. Strasters, "Restoration of confocal images for quantitative image analysis," J. Microsc. **178**, 165–181 (1995).
3. W. A. Carrington, "Image restoration in 3D microscopy with limited data," in *Bioimaging and Two-Dimensional Spectroscopy*, L. C. Smith, ed., Proc. SPIE **1205**, 72–83 (1990).
4. W. A. Carrington, R. M. Lynch, E. M. Moore, G. Isenberg, K. E. Fogarty, and F. S. Fay, "Superresolution three-dimensional images of fluorescence in cells with minimal light exposure," Science **268**, 1483–1487 (1995).
5. T. J. Holmes, "Maximum-likelihood image restoration adapted for noncoherent optical imaging," J. Opt. Soc. Am. A **5**, 666–673 (1988).
6. G. M. P. van Kempen, "Image restoration in fluorescence microscopy," Ph.D. Thesis (Delft University of Technology, Delft, The Netherlands, 1999).
7. A. P. Dempster, N. M. Laird, and D. B. Rubin, "Maximum likelihood from incomplete data via the EM algorithm," J. R. Stat. Soc. B Sect. **39**, 1–37 (1977).
8. Y. Vardi, L. A. Shepp, and L. Kaufman, "A statistical model for positron emission tomography," J. Am. Stat. Assoc. **80**, 8–35 (1985).
9. L. A. Shepp and Y. Vardi, "Maximum likelihood reconstruction for emission tomography," IEEE Trans. Med. Imaging **MI-1**, 113–121 (1982).
10. D. L. Snyder, A. M. Hammoud, and R. L. White, "Image recovery from data acquired with a charge-coupled-device camera," J. Opt. Soc. Am. A **10**, 1014–1023 (1993).
11. G. M. P. van Kempen, L. J. van Vliet, P. J. Verveer, and H. T. M. van der Voort, "A quantitative comparison of image restoration methods for confocal microscopy," J. Microsc. **185**, 354–365 (1997).
12. W. H. Richardson, "Bayesian-based iterative method of image restoration," J. Opt. Soc. Am. **62**, 55–59 (1972).
13. R. W. Gerchberg, "Super-resolution through error energy reduction," Opt. Acta **14**, 709–720 (1979).
14. A. K. Jain, *Fundamentals of Digital Image Processing, Vol. IP* (Prentice Hall, Englewood Cliffs, N.J., 1989).
15. J.-A. Conchello, "Superesolution and convergence properties of the expectation-maximization algorithm for maximum-likelihood deconvolution of incoherent images," J. Opt. Soc. Am. A **15**, 2609–2619 (1998).
16. J.-A. Conchello and J. G. McNally, "Fast regularization technique for expectation maximization algorithm for optical sectioning microscopy," presented at the conference on Three-Dimensional Microscopy: Image Acquisition and Processing III, San Jose, Calif., February 1–3, 1996.
17. H. C. Andrews and B. R. Hunt, *Digital Image Restoration* (Prentice-Hall, Englewood Cliffs, N.J., 1977).
18. M. Bertero and P. Boccacci, *Introduction to Inverse Problems in Imaging* (IOP, London, 1998).
19. L. J. van Vliet, D. Sudar, and I. T. Young, "Digital fluorescence imaging using cooled charge-coupled device array cameras," in *Cell Biology: A Laboratory Handbook*, 2nd ed., J. E. Celis, ed. (Academic, London, 1998), Vol. 3, pp. 109–120.
20. J. Art, "Photon detectors for confocal microscopy," in *Handbook of Biological Confocal Microscopy*, J. B. Pawley, ed. (Plenum, New York, 1995), pp. 183–196.
21. A. N. Tikhonov and V. Y. Arsenin, *Solutions of Ill-Posed Problems* (Wiley, New York, 1977).
22. T. Wilson and J. B. Tan, "Three dimensional image reconstruction in conventional and confocal microscopy," Bioimaging **1**, 176–184 (1993).

23. G. M. P. van Kempen, L. J. van Vliet, and P. J. Verveer, "Application of image restoration methods for confocal fluorescence microscopy," presented at the conference on Three-Dimensional Microscopy: Image Acquisition and Processing IV, San Jose, Calif., February 12–13, 1997.
24. P. J. Verveer, M. J. Gemkow, and T. M. Jovin, "A comparison of image restoration approaches applied to three-dimensional confocal and wide-field fluorescence microscopy," J. Microsc. **193**, 50–61 (1999).
25. P. J. Verveer and T. M. Jovin, "Acceleration of the ICTM image restoration algorithm," J. Microsc. **188**, 191–195 (1997).
26. W. H. Press, S. A. Teukolsky, W. T. Vetterling, and B. P. Flannery, *Numerical Recipes in C*, 2nd ed., Vol. CS (Cambridge U. Press, Cambridge, UK, 1992).
27. W. A. Carrington and K. E. Fogarty, "3-D molecular distribution in living cells by deconvolution of optical sections using light microscopy," presented at the 13th Annual Northeast Bioengineering Conference, Philadelphia, Pa., March 12–13, 1987.
28. D. L. Snyder and M. I. Miller, *Random Point Processes in Time and Space*, Vol. SP (Springer Verlag, Berlin, 1991).
29. K. M. Perry and S. J. Reeves, "Generalized cross-validation as a stopping rule for the Richardson–Lucy algorithm," presented at the conference on Restoration of HST Images and Spectra II, Baltimore, Md., November 18–19, 1993.
30. P. W. Verbeek, H. A. Vrooman, and L. J. van Vliet, "Low-level image processing by max-min filters," Signal Process. **15**, 249–258 (1988).
31. I. T. Young, "Automated Leukocyte Recognition," in *Automated Cell Identification and Cell Sorting*, G. L. Wied and G. F. Bahr, eds. (Academic, New York, 1970), pp. 187–194.
32. I. Heertje, E. C. Roijers, and H. A. C. M. Hendrickx, "Liquid crystalline phases in the structuring of food products," Lebensm.-Wiss. Technol. **31**, 387–396 (1998).
33. G. M. P. van Kempen, N. van den Brink, L. J. van Vliet, M. van Ginkel, P. W. Verbeek, and H. Blonk, "The application of a local dimensionality estimator to the analysis of 3-D microscopic network structures," presented at the 11th Scandinavian Conference on Image Analysis, Kangerlussuaq, Greenland, June 7–11, 1999.
34. P. J. Verveer, "Computational and optical methods for improving resolution and signal quality in fluorescence microscopy," Ph.D. thesis (Delft University of Technology, Delft, The Netherlands, 1998).
35. G. Demoment, "Image reconstruction and restoration: overview of common estimation structures and problems," IEEE Trans. Acoust., Speech, Signal Process. **37**, 2024–2036 (1989).